RSC Advances

PAPER

View Article Online
View Journal | View Issue

Cite this: *RSC Adv.*, 2017, **7**, 35558

Lightweight, interconnected VO_2 nanoflowers hydrothermally grown on 3D graphene networks for wide-voltage-window supercapacitors†

Junya Wang,[a] Xuetao Zhang,[a] Yue Zhang,[a] Asim Abas,[a] Xiaohua Zhao,[a] Zhiwei Yang,[a] Qing Su,[a] Wei Lan *[ab] and Erqing Xie [a]

Received 18th April 2017
Accepted 12th July 2017

DOI: 10.1039/c7ra04376g

rsc.li/rsc-advances

Highly stable and interconnected VO_2 nanoflowers were uniformly grown on flexible three dimensional graphene networks, which directly served as a lightweight and high conductivity supercapacitor electrode (VO_2 NF@3DG). The uniform VO_2 NF@3DG hybrid provided direct and stable pathways for rapid electron and ion transport. The hybrid produced an improved areal specific capacitance of 466 mF cm^{-2} and 283.2 mF cm^{-2} for the three- and the two-electrode configurations, respectively. A capacitance retention of 63.5% after 3000 cycles showed that the VO_2 NF@3DG hybrid had a stable cycling performance at a high specific capacitance. A high energy density of 279.6 mW h m^{-2} and a high power density of 60 000 mW m^{-2} were achieved in symmetrical supercapacitors. The effective strategy could be applied to improve the performance of supercapacitors with high efficiency, wide potential windows and long life.

1. Introduction

Energy storage technologies have attracted global attention emanating from the ever-growing demands for renewable energy and the environmental crisis. Supercapacitors, as an essential energy storage device, have been studied because of their high-power density, long cycle life and fast charge/discharge rate.[1–3] Typically, supercapacitors can be classified as electric double-layer capacitors (EDLCs) and pseudocapacitors.[4–6] Pseudocapacitors with metal oxide or conducting polymer electrodes offer a better capacitive behavior, and store energy by employing a fast-reversible redox reaction at the interfaces between the electrodes and electroactive species in the electrolyte.[7–9] In general, the most important factor is the electrode materials, which influence the capacitive behavior of supercapacitors. Various transition-metal oxides have been studied as electrode materials for pseudocapacitors, such as MoO_3,[10] MnO_2,[11] Fe_2O_3,[12] VO_2,[13] and Co_3O_4.[14]

Among various oxides, vanadium oxides has been suggested as one of the most promising pseudocapacitance electrode materials due to its high energy density, low cost, and wide potential windows, arising from vanadium multivalent states (V^{2+}, V^{3+}, V^{4+}, and V^{5+}).[15,16] Based on the basic principle of energy storage, the nanostructures of vanadium oxides become an inevitable way to improve the performance of supercapacitors. The various nanostructures of vanadium oxides for supercapacitors had been realized, such as nanobelts,[17] nanoflakes,[18] nanowires,[19] nanotextiles.[20] However, vanadium oxides did not usually deliver ideal specific capacitance behavior because of its low electrical conductivity and the poor structural stability.[21] Therefore, a strategy has been employed to be a hybrid by introducing excellent conductive materials with high structure stability into vanadium oxides, such as graphene. Graphene has a unique superior electrical conductivity, large specific surface area, high mechanical flexibility and chemical stability.[22]

In this work, three dimensional graphene (3DG) networks grown by chemical vapor deposition (CVD) acted as a current collector, VO_2 nanoflowers were hydrothermally anchored on 3DG networks (VO_2 NF@3DG) using dodecylamine as a reducing agent. As a binder-free, conductive-agent-free and self-supported supercapacitor electrode, the VO_2 NF@3DG hybrid had been investigated the electrochemical performances in detail. The results showed that the VO_2 NF@3DG electrode possessed high areal specific capacity (466 mF cm^{-2}), outstanding cycling stability (the retention of 63.5% after 3000 cycles) and high energy densities (279.6 mW h m^{-2}).

2. Experimental section

A schematic diagram of preparation process for the VO_2 NF@3DG hybrid electrode was illustrated in Fig. 1. Above all, 3DG was synthesized by CVD technique, which had been

[a]*a Key Laboratory of Special Function Materials and Structure Design, Ministry of Education, School of Physical Science and Technology, Lanzhou University, Lanzhou, 730000, People's Republic of China. E-mail: lanw@lzu.edu.cn*

[b]*State Key Laboratory of Advanced Processing and Recycling of Non-Ferrous Metals, Lanzhou University of Technology, Lanzhou, 730050, People's Republic of China*

† Electronic supplementary information (ESI) available. See DOI: 10.1039/c7ra04376g

described in our previous reports.[23,24] In brief, Ni foam slice (110 pores per inch, ~380 g m^{-2} and ~1.5 mm thick, pressed to ~0.5 mm) was heated up to 1000 °C in a tube furnace under H_2/Ar ambience. Ethanol was introduced by flowing H_2/Ar (20 sccm/100 sccm) gas to the furnace under atmospheric pressure. After 20 min reaction, the quartz tube was quickly cooled down to room temperature, 3DG grown on Ni foam slice was obtained. Afterwards, the samples were eliminated by 3 M HCl aqueous solution for 6 h at 60 °C to gain lightweight free-supported 3DG networks.

VO_2 nanoflowers were synthesized on 3DG networks by a simple hydrothermal method. Initially, 0.5 g of V_2O_5 was dissolved in 25 ml deionized water followed by slow addition of 25 ml hydrogen peroxide (30%) solution with strongly string for 3 h at 0 °C. The resultant solution ($V_2O_5 \cdot nH_2O$) was obtained after standing at ambient temperature for 12 hours. In this process, the chemical reactions was as follows:

$$V_2O_5 + H_2O_2 \rightarrow 2HVO_4 + H_2O \quad (1)$$

$$HVO_4 + (n-1)H_2O \rightarrow V_2O_5 \cdot nH_2O + O_2 \quad (2)$$

Then, 0.255 g of dodecylamine was dissolved in 2 ml ethanol with strongly string for 1 h and added drop wise to the above-prepared solution. The resultant solution was stirred for 24 hours at 0 °C, and then transferred into a 50 ml Teflon-liner autoclave within a piece of 3DG networks. The reaction was completed at 180 °C for different time (12, 24, 36, 48 h). Finally, the samples were washed with deionized water for several times, dried at 60 °C for 8 h. The lightweight VO_2 NF@3DG hybrid were obtained.

The morphology of the samples was characterized by field emission scanning electron microscopy (FE-SEM, TESCAN MIRA3 XMU). The microstructure was characterized using high resolution transmission electron microscopy (HRTEM, FEI Tecnai F30, operated at 300 kV). The crystal structures were examined by X-ray diffraction (XRD, Philips, X'pert pro, Cu Kα, 0.154056 nm) and Raman spectroscopy (JY-HR800 micro-Raman, using a 532 nm wavelength YAG laser with a laser spot diameter of ~600 nm). The mass of active materials was measured by a microbalance (Mettler Toledo, XSE) with an accuracy of 0.01 mg. The loaded quantity was obtained by the mass difference of the samples between the before and the after hydrothermal reaction. The mass of VO_2 nanoflowers on 3D graphene was around 0.91 mg cm^{-2}. 3DG has the mass density of ~8.22 mg cm^{-2}. Electrochemical measurements (CHI 660E) were accomplished in three-electrode and two-electrode configurations at room temperature in a 0.5 M K_2SO_4 aqueous electrolyte. A platinum sheet was used as counter electrode, and a saturated calomel electrode (SCE) was used as reference electrode. The VO_2 NF@3DG hybrid was directly utilized as the working electrode. The nominal area of the VO_2 NF@3DG hybrid immersed into the electrolyte was controlled to be around 1 cm × 1 cm. Electrochemical impedance spectroscopy (EIS) was applied with 5 mV AC perturbation amplitude in the frequency range from 1 MHz to 0.01 Hz. The areal-specific capacitance (C_a, mF cm^{-2}) of the three-electrode configuration was calculated by the following equation.

$$C_a = \frac{It}{S\Delta V} \quad (3)$$

where, I is the charge–discharge current (A), t is the discharge time (s), S is the electrode area and ΔV is the potential (V).

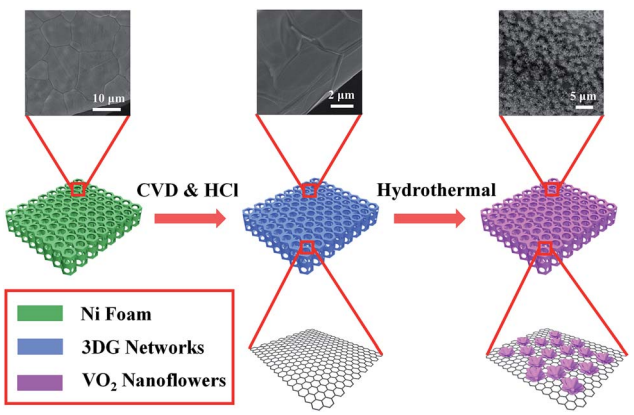

Fig. 1 The schematic diagram of preparation process for VO_2 NF@3DG hybrid.

3. Results and discussion

Fig. 1 shows the schematic diagram of preparation for VO_2 NF@3DG hybrid, which demonstrates the two procedures, including the growth of lightweight self-supported 3DG networks by combining CVD and HCl corrosion, and the anchoring of VO_2 nanoflowers by hydrothermal process. Fig. 2 shows the typical SEM and TEM images of VO_2 nanoflowers, which are interconnected and distributed on 3DG networks. (1) The nanoflowers were made of small VO_2 nanobelts. Fig. S1† shows the SEM images of VO_2 nanoflowers grown at different hydrothermal time. More details can be seen in the high-resolution TEM image in Fig. 2d. The lattice fringe with a spacing distance of 0.186 nm was indexed to the (312) crystal planes of VO_2 phase (JCPDS card no. 31-1438). Fig. 2e shows the crystal phase and structure information of the VO_2 NF@3DG hybrid, VO_2 NF and 3DG. The XRD peaks of VO_2 NF were all indexed to VO_2 phase (JCPDS card no. 31-1438). A sharp diffraction peak located at 49.496° was clearly visible and assigned to VO_2 (312) reflections, which was consistent with the HRTEM result. Therefore, VO_2 NF@3DG hybrid has been prepared successfully. The micro-zone Raman spectra of VO_2 NF@3DG hybrid, VO_2 NF and 3DG have been shown in Fig. 2f. The Raman spectrum of VO_2 NF displayed the bending vibrations of V=O, the triply coordinated oxygen of V_3–O, the doubly coordinated oxygen of V_2–O and terminal V=O bond, which were identified to the Raman-shift peaks of 183, 265, 527, 693 and 923 cm^{-1}.[13,25] The Raman spectrum of 3DG networks shows a G peak at 1580 cm^{-1} and a 2D peak at 2716 cm^{-1}. The G peak originated from the vibration of carbon atoms in the hexagonal graphene lattice, and the 2D peak corresponded to the second order of zone-boundary phonons. The lack of D peak for graphene suggested few defects and the high quality 3DG

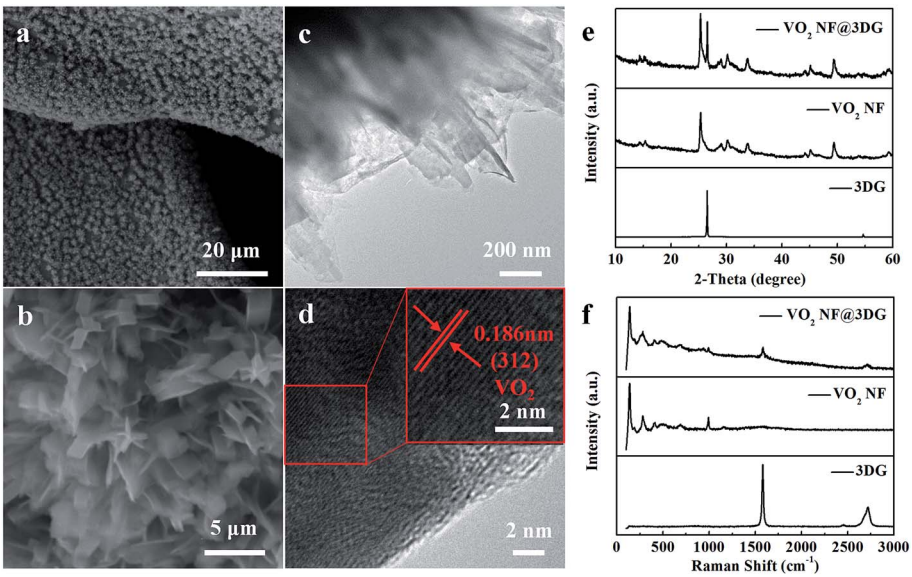

Fig. 2 (a, b) SEM and (c, d) TEM images of VO_2 NF@3DG hybrid. (e) XRD pattern and (f) micro-zone Raman spectrum of VO_2 NF@3DG hybrid, VO_2 NF and 3DG.

networks, which could shorten transport paths for ions and electrons, amplify the contact area with electrolyte, and then elevate the utilization of VO_2 pseudo-capacitance materials.[26,27]

A typical XPS spectrum for the VO_2 NF@3DG hybrid (Fig. 3a) indicates the existence of C, O and V elements. The high-resolution XPS spectrum for C can be deconvoluted into three peaks (Fig. 3b), where the peaks at 284.8, 286 and 288.5 eV correspond to the reported binding energy for C–O (sp^2-hybridized carbon), C–O and C=O.[28,29] The corresponding O1s spectrum is shown in Fig. 3b. The O1s spectrum is broad and asymmetric, which can be deconvoluted into three peaks, indicating the existence of three different oxygen species. The peaks located at the binding energy of 530, 531 eV are attributed to the V–O linkage of VO_2 and V_2O_5, while the peaks at 532.2 is due to OH^-.[30,31] The $V2p_{3/2}$ spectrum can be deconvoluted into two peaks (Fig. 3d), where the peaks at 516.3 and 517.2 eV correspond to the reported binding energy of $V2p_{3/2}$ for V^{4+} and V^{5+}, respectively.[32] The $V2p_{1/2}$ peak is located at 524.1 eV. The existence of V^{5+} might result from the surface oxidation of the samples in air. The same phenomenon had also been reported

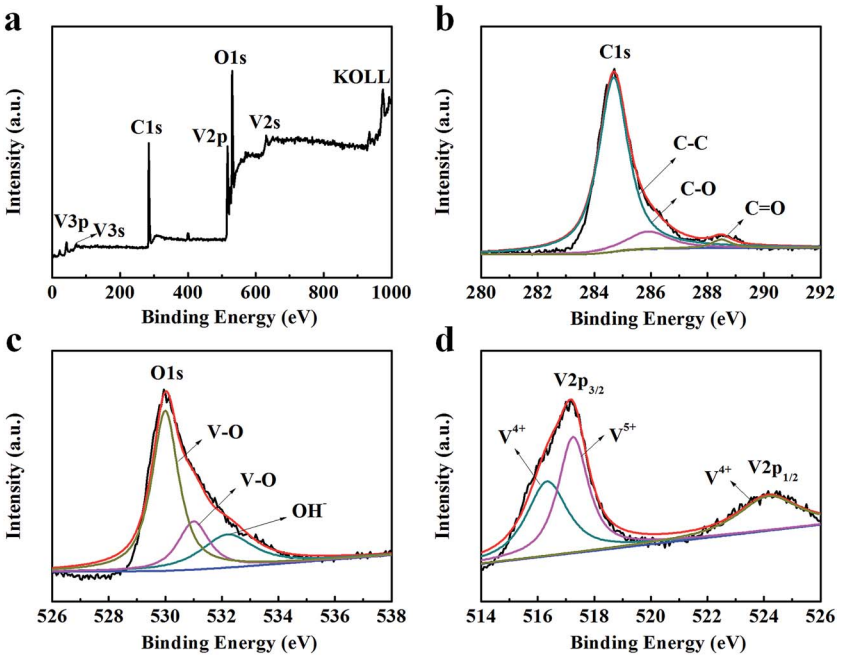

Fig. 3 XPS spectra of VO_2 NF@3DG hybrid. (a) Survey spectrum. High-resolution XPS spectra of (b) C, (c) O and (d) V element.

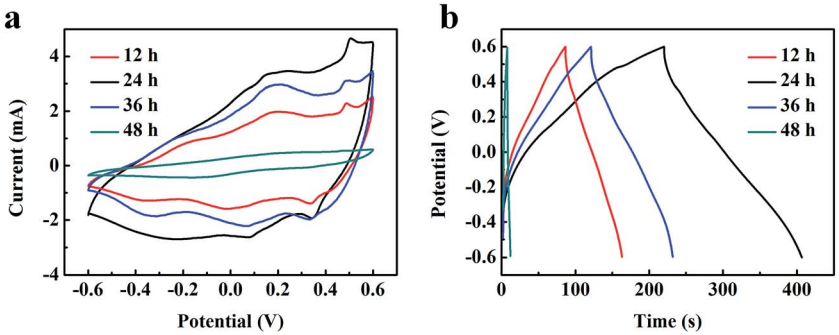

Fig. 4 (a) CV and (b) GCD curves of VO_2 NF@3DG hybrid electrodes prepared at different hydrothermal time (12, 24, 36 and 48 h).

by other groups.[31,33] These results further proved that the nanostructures of VO_2 had been successfully grown on the surface of graphene.

Electrochemical measurements were carried out to verify the potential application of VO_2 NF@3DG electrode materials. Fig. 4a shows typical cyclic voltammetry (CV) curves of VO_2 NF@3DG hybrids prepared at different hydrothermal time (12, 24, 36, and 48 h). It can be clearly seen that the CV curves, at the scan rate of 5 mV s^{-1}, exhibit an approximate rectangular shape with small redox peaks. Fig. S2† shows the CV curves of VO_2 NF@3DG hybrids and 3DG electrodes. These indicated the faradaic pseudocapacitance behaviors of the hybrid electrodes, which were caused by the electrochemical K^+ insertion procedure as follows:[13,34]

$$VO_2 + xK^+ + xe^- \leftrightarrow 4K_xVO_2 \quad (4)$$

In terms of the area of CV curves, related to the capacitance value, the VO_2 NF@3DG synthesized for 24 h had the larger, which represented the more excellent capacitance behavior. Fig. 4b showed galvanostatic charge–discharge (GCD) curves of VO_2 NF@3DG electrodes synthesized at different hydrothermal time with a current density of 3 mA cm^{-2}. The areal specific capacitances of VO_2 NF@3DG hybrid electrodes at different hydrothermal time (12, 24, 36, and 48 h) were 11.3, 466.5, 277.5, 192.5 mF cm^{-2} respectively. All the results indicated that the VO_2 NF@3DG hybrid with hydrothermal 24 h had the most excellent electrochemical performance. So the VO_2 NF@3DG hybrid grown for 24 h was further investigated in the following.

Fig. 5a showed the CV curves of VO_2 NF@3DG hybrid prepared for 24 h at different sweep rates. The capacitive current was enhanced with the increased scan rate, indicating an excellent electrochemical reversibility and the fast diffusion of the electrolyte ions into the VO_2 NF@3DG hybrid electrode. The GCD was carried out at different current densities (Fig. 5b).

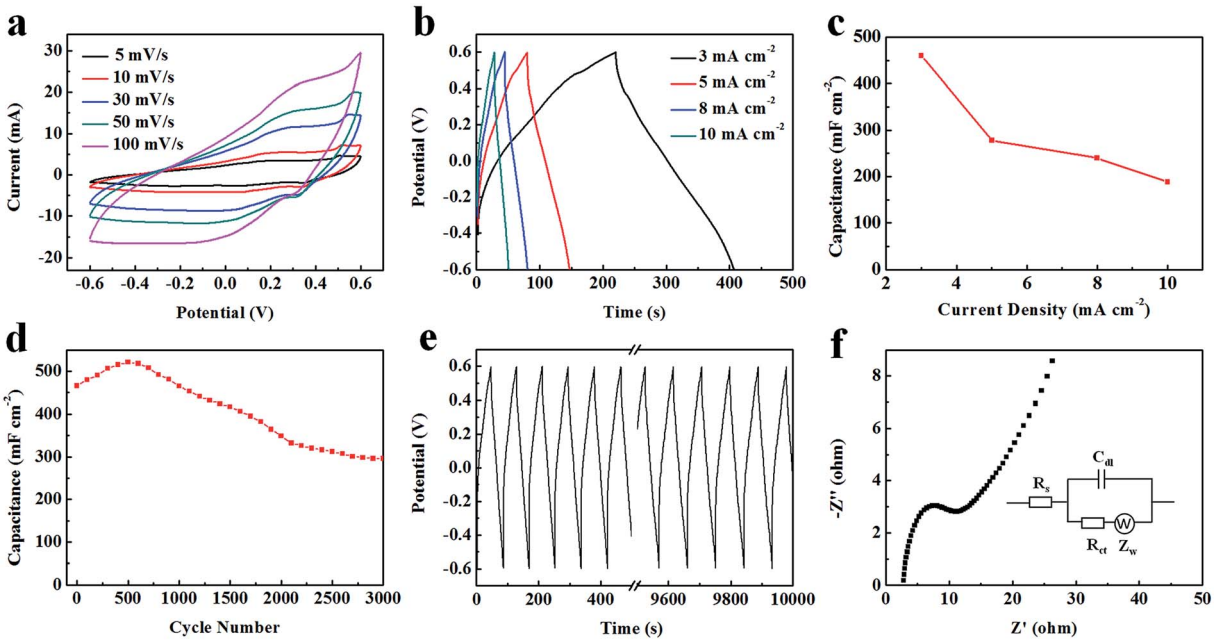

Fig. 5 (a) CV and (b) GCD curves of VO_2 NF@3DG hybrid electrode, (c) the areal specific capacitance of VO_2 NF@3DG as a function of current density. (d) Electrochemical cycling performance, and (e) the charge–discharge curves during electrochemical cycling process of VO_2 NF@3DG hybrid. (f) Nyquist plot and equivalent circuit diagram (the inset) of VO_2 NF@3DG hybrid.

The calculated areal capacitance Ca of VO_2 NF@3DG hybrid was 466 mF cm^{-2} (507 F g^{-1}), 278 mF cm^{-2} (302 F g^{-1}), 240 mF cm^{-2} (261 F g^{-1}), 191 mF cm^{-2} (208 F g^{-1}) at 3, 5, 8, 10 mA cm^{-2}, respectively (Fig. 5c). The ~41% Ca was remained with the increasing current density from 3 to 10 mA cm^{-2}. The rate performance was better than the reported results. Nie *et al.* obtained 27.3% rate capability of VO_2@PANi coaxial nanobelts (from 0.5 A g^{-1} to 5.0 A g^{-1}),[25] Zheng *et al.* fabricated V_2O_3@C core–shell composites and get 32.3% rate performance (0.1 A g^{-1} to 10 A g^{-1}).[35] Li *et al.* obtained the rate of 39% for rGO coated V_2O_5 microspheres (from 1 A g^{-1} to 20 A g^{-1}) as the supercapacitor electrodes.[36]

Electrochemical cycle of VO_2 NF@3DG hybrid electrode was further carried out, which was shown in Fig. 5e, with the increase of cycles, the areal-specific capacitance remained 63.5% after 3000 cycles, compared to the initial Ca (466 mF cm^{-2}), which reflected a good cycling performance of VO_2 NF@3DG hybrid electrode. The increase of the Ca at first 500 cycles could be due to the improved wettability and activation process of the electrodes. In Table 1, our results are compared with other results on the electrochemical performances of supercapacitor electrodes.[13,25,36–40] It can be clearly seen that the capacitance and cycle stability of the VO_2 NF@3DG hybrid electrode are comparable or better than those in other works. What's more, as seen from the EIS curve (Fig. 5f), the intersection of the curve at the real axis indicates the resistance of the electrochemical system at the high frequency, and the semicircle diameter reflects the charge-transfer resistance (R_{ct}).[41,42] Through calculating, the equivalent series resistance (R_s) was a low value of 2.918 Ω, and the R_{ct} value was 0.468 Ω. In the low frequency range, the slope of the curve approaching 90° suggests negligible diffusive resistance for the VO_2 NF@3DG hybrid. Therefore, these results confirms that the VO_2 NF@3DG hybrid as the supercapacitor electrode has excellent electrochemical performances.

To check the practical electrochemical behaviors of the VO_2 NF@3DG hybrid in devices, a symmetrical supercapacitor was assembled by using two pieces of VO_2 NF@3DG hybrids. Fig. 6a shows typical CV curves of two-electrode configuration at various scan rates for potentials between −0.6 and 0.6 V. The obtained CV curves exhibit rectangular-like shapes without obvious redox peaks, indicating an ideal capacitive behavior. The GCD measurements at different current densities were measured and shown in Fig. 6b. Herein, the areal-specific capacitance (C_{as}, mF cm^{-2}), energy density (E), and power density (P) of the two-electrode configuration were calculated according to the eqn (5)–(7), respectively.[43,44]

$$C_{as} = \frac{It}{S\Delta V} \quad (5)$$

$$E = \frac{1}{2} C_{as} (\Delta V)^2 \quad (6)$$

$$P = \frac{E}{t} \quad (7)$$

The supercapacitor device exhibited an areal specific capacitance of 70.8 mF cm^{-2} at 0.5 mA cm^{-2}. The calculated results are shown in the Ragone plots (Fig. 6c). It is found that the symmetrical supercapacitors exhibits a high energy density of

Table 1 The electrochemical performance comparison of our results with other works

Material	Electrolyte	Current density	Specific capacitance	Stability (cycle)	Ref.
V_4O_9 yolk–shell microspheres	1.5 M KOH	0.5 A g^{-1}	392 F g^{-1}	75% (2000)	37
VO_2@PANi nanobelts	0.5 M Na_2SO_4	0.5 A g^{-1}	246 F g^{-1}	28.6% (1000)	25
Graphene/VO_2 nanobelts	0.5 M K_2SO_4	1 A g^{-1}	426 F g^{-1}	82% (5000)	13
Graphene/VO_2 particles	0.5 M K_2SO_4	0.25 A g^{-1}	225 F g^{-1}	81% (1000)	38
Graphene/VO_x nanotubes	1 M Na_2SO_4	1 A g^{-1}	210 F g^{-1}	48% (5000)	39
V_2O_5 3D nanosheets	1 M Na_2SO_4	0.5 A g^{-1}	451 F g^{-1}	90% (4000)	40
V_2O_5 microspheres/rGO	8 M LiCl	1 A g^{-1}	537 F g^{-1}	84% (1000)	36
VO_2 nanoflowers@3DG	0.5 M K_2SO_4	~3.3 A g^{-1}	507 F g^{-1}	63.5% (3000)	Our work

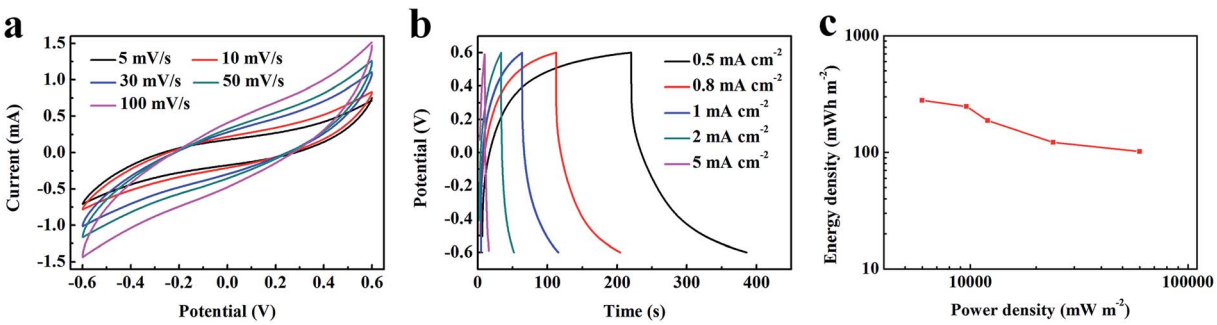

Fig. 6 (a) CV curves, (b) GCD curves and (c) Ragone plot of the symmetrical supercapacitor device assembled by two pieces of VO_2 NF@3DG hybrids.

279.6 mW h m^{-2} at a power density of 6000 mW m^{-2} and a high power density of 60 000 mW m^{-2} at a energy density of 102 mW h m^{-2}. Therefore, the measurement results in two-electrode configuration have proved the possibility of the practical application for the VO_2 NF@3DG hybrid as the supercapacitor electrode.

4. Conclusions

In this work, the lightweight, flexible and interconnected VO_2 nanoflowers was successfully grown on 3DG networks with high specific surface area and high conductivity, directly served as supercapacitor electrodes. The large specific capacitance (466 mF cm^{-2}), long cycling stability (63.5% after 3000 cycles), high energy density (279.6 mW h m^{-2}) and high power density (60 000 mW m^{-2}) were achieved in the VO_2 NF@3DG hybrid electrodes. This study provides an effective strategy to improve the performance of electrode materials for supercapacitors with a wide potential windows and long life, which makes them promising candidates for future energy-storage applications.

Acknowledgements

This work was supported by Natural Science Foundation of Gansu Province (No. 1208RJZA199), the fund of the State Key Laboratory of Advanced Processing and Recycling of Non-ferrous Metals, Lanzhou University of Technology (SKLAB02014003), the Fundamental Research Funds for the Central Universities (lzujbky-2017-k21), and the Project-sponsored by SRF for ROCS, SEM.

References

1 E. Frackowiak and F. Béguin, Carbon materials for the electrochemical storage of energy in capacitors, *Carbon*, 2001, **39**, 937–950.
2 Y. Zhu, S. Murali, M. D. Stoller, K. J. Ganesh, W. Cai, P. J. Ferreira, A. Pirkle, R. M. Wallace, K. A. Cychosz, M. Thommes, D. Su, E. A. Stach and R. S. Ruoff, Carbon-based supercapacitors produced by activation of graphene, *Science*, 2011, **332**, 1537–1541.
3 F. Béguin, V. Presser, A. Balducci and E. Frackowiak, Carbons and electrolytes for advanced supercapacitors, *Adv. Mater.*, 2014, **26**, 2219–2251.
4 F. Wolfart, D. P. Dubal, M. Vidotti and P. Gómez-Romero, Hybrid core–shell nanostructured electrodes made of polypyrrole nanotubes coated with $Ni(OH)_2$ nanoflakes for high energy-density supercapacitors, *RSC Adv.*, 2016, **6**, 15062–15070.
5 S. Liu, K. S. Hui and K. N. Hui, Flower-like Copper Cobaltite Nanosheets on Graphite Paper as High-Performance Supercapacitor Electrodes and Enzymeless Glucose Sensors, *ACS Appl. Mater. Interfaces*, 2016, **8**, 3258–3267.
6 S. Zhang, H. Gao, M. Huang and J. Zhou, One-step hydrothermal synthesis of nitrogen doping graphene based cobalt oxide and its supercapacitive properties, *J. Alloys Compd.*, 2017, **705**, 801–805.
7 J. Patiño, N. López-Salas, M. C. Gutiérrez, D. Carriazo and M. L. Ferrer, Phosphorus-doped carbon–carbon nanotube hierarchical monoliths as true three-dimensional electrodes in supercapacitor cells, *J. Mater. Chem. A*, 2016, **4**, 1251–1263.
8 X. T. Hong, K. S. Hui, Z. Zeng, K. N. Hui, L. J. Zhang, M. Y. Mo and M. Li, Hierarchical nitrogen-doped porous carbon with high surface area derived from endothelium corneum gigeriae galli for high-performance supercapacitor, *Electrochim. Acta*, 2014, **130**, 464–469.
9 Y. Qian, R. Liu, Q. F. Wang, J. Xu, D. Chen and G. Z. Shen, Efficient synthesis of hierarchical NiO nanosheets for high-performance flexible all-solid-state supercapacitors, *J. Mater. Chem. A*, 2014, **2**, 10917–10922.
10 Q. Mahmood, H. J. Yun, W. S. Kim and H. S. Park, Highly uniform deposition of MoO_3 nanodots on multiwalled carbon nanotubes for improved performance of supercapacitors, *J. Power Sources*, 2013, **235**, 187–192.
11 L. Yuan, X. H. Lu, X. Xiao, T. Zhai, J. Dai, F. Zhang, B. Hu, X. Wang, L. Gong, J. Chen, C. Hu, Y. Tong, J. Zhou and Z. Wang, Flexible solid-state supercapacitors based on carbon nanoparticles/MnO_2 nanorods hybrid structure, *ACS Nano*, 2012, **6**, 656–661.
12 C. Guan, J. Liu, Y. Wang, L. Mao, Z. Fan, Z. Shen, H. Zhang and J. Wang, Iron oxide-decorated carbon for supercapacitor anodes with ultrahigh energy density and outstanding cycling stability, *ACS Nano*, 2015, **9**, 5198–5207.
13 H. Wang, H. Yi, X. Chen and X. Wang, One-step strategy to three-dimensional graphene/VO_2 nanobelt composite hydrogels for high performance supercapacitors, *J. Mater. Chem. A*, 2014, **2**, 1165–1173.
14 J. Wang, W. Dou, X. Zhang, W. Han, X. Mu, Y. Zhang, X. Zhao, Y. Chen, Z. Yanga, Q. Su, E. Xie, W. Lan and X. Wang, Embedded Ag quantum dots into interconnected Co_3O_4 nanosheets grown on 3D graphene networks for high stable and flexible supercapacitors, *Electrochim. Acta*, 2017, **224**, 260–268.
15 Q. Qu, Y. Zhu, X. Gao and Y. Wu, Core–shell structure of polypyrrole grown on V_2O_5 nanoribbon as high performance anode material for supercapacitors, *Adv. Energy Mater.*, 2012, **2**, 950–955.
16 D. J. Yan, X. D. Zhu, K. X. Wang, X. T. Gao, Y. J. Feng, K. N. Sun and Y. T. Liu, Facile and elegant self-organization of Ag nanoparticles and TiO_2 nanorods on V_2O_5 nanosheets as a superior cathode material for lithium-ion batteries, *J. Mater. Chem. A*, 2016, **4**, 4900–4907.
17 M. Lee, B. H. Wee and J. D. Hong, High Performance Flexible Supercapacitor Electrodes Composed of Ultralarge Graphene Sheets and Vanadium Dioxide, *Adv. Energy Mater.*, 2015, **5**, 1401890.
18 X. Xia, D. Chao, C. F. Ng, J. Lin, Z. Fan, H. Zhang, Z. Shen and H. Fan, VO_2 nanoflake arrays for supercapacitor and Li-ion battery electrodes: performance enhancement by hydrogen molybdenum bronze as an efficient shell material, *Mater. Horiz.*, 2015, **2**, 237–244.
19 X. T. Gao, X. D. Zhu, S. R. Le, D. J. Yan, C. Y. Qu, Y. J. Feng and Y. T. Liu, Boosting High-Rate Lithium Storage of V_2O_5

Nanowires by Self-Assembly on N-Doped Graphene Nanosheets, *ChemElectroChem*, 2016, **3**, 1730–1736.

20 Y. L. Ding, Y. Wen, C. Wu, P. A. van Aken, J. Maier and Y. Yu, 3D V_6O_{13} nanotextiles assembled from interconnected nanogrooves as cathode materials for high-energy lithium ion batteries, *Nano Lett.*, 2015, **15**, 1388–1394.

21 T. Qian, N. Xu, J. Zhou, T. Yang, X. Liu, X. Shen, J. Liang and C. Yan, Interconnected three-dimensional V_2O_5/polypyrrole network nanostructures for high performance solid-state supercapacitors, *J. Mater. Chem. A*, 2015, **3**, 488–493.

22 A. Geim, Graphene: status and prospects, *Science*, 2009, **324**, 1530–1534.

23 W. Deng, W. Lan, Y. Sun, Q. Su and E. Xie, Porous CoO nanostructures grown on three-dimension graphene foams for supercapacitors electrodes, *Appl. Surf. Sci.*, 2014, **305**, 433–438.

24 W. Lan, Y. Sun, Y. Chen, J. Wang, G. Tang, W. Dou and E. Xie, Ultralight and flexible supercapacitor electrodes made from $Ni(OH)_2$ nanosheets doped with Ag nanoparticle/3D graphene composite, *RSC Adv.*, 2015, **5**, 20878–20883.

25 G. Nie, X. Lu, Y. Zhu, M. Chi, M. Gao, S. Chen, M. Chi and C. Wang, Reactive Template Synthesis of Inorganic/Organic VO_2@Polyaniline Coaxial Nanobelts for High-Performance Supercapacitors, *ChemElectroChem*, 2017, **4**, 1095–1100.

26 S. J. Chae, F. Guenes, K. K. Kim, E. S. Kim and G. H. Han, Synthesis of large-area graphene layers on poly-nickel substrate by chemical vapor deposition: wrinkle formation, *Adv. Mater.*, 2009, **21**, 2328–2333.

27 A. C. Ferrari, J. C. Meyer, V. Scardaci, C. Casiraghi, M. Lazzeri and F. Mauri, Raman spectrum of graphene and graphene layers, *Phys. Rev. Lett.*, 2006, **97**, 187401.

28 C. Zhu, S. Guo, Y. Fang and S. Dong, Reducing sugar: new functional molecules for the green synthesis of graphene nanosheets, *ACS Nano*, 2010, **4**, 2429–2437.

29 S. Stankovich, D. Dikin, R. Piner, K. Kohlhaas, A. Kleinhammes, Y. Jia, Y. Wu, S. Nguyen and R. Ruoff, Synthesis of graphene-based nanosheets *via* chemical reduction of exfoliated graphite oxide, *Carbon*, 2007, **45**, 1558–1565.

30 M. Sathiya, A. Prakash, K. Ramesha, J.-M. Tarascon and A. Shukla, V_2O-anchored carbon nanotubes for enhanced electrochemical energy storage, *J. Am. Chem. Soc.*, 2011, **133**, 16291–16299.

31 C. Hu, H. Xu, X. Liu, F. Zou, L. Qie, Y. Huang and X. Hu, VO_2/TiO_2 nanosponges as binder-free electrodes for high-performance supercapacitors, *Sci. Rep.*, 2015, **5**, 16012.

32 T. Zhai, X. Lu, Y. Ling, M. Yu, G. Wang, T. Liu and Y. Li, A New Benchmark Capacitance for Supercapacitor Anodes by Mixed-Valence Sulfur-Doped V_6O_{13-x}, *Adv. Mater.*, 2014, **26**, 5869–5875.

33 N. Alov, D. Kutsko, I. Spirovová and Z. Bastl, XPS study of vanadium surface oxidation by oxygen ion bombardment, *Surf. Sci.*, 2006, **600**, 1628–1631.

34 X. J. Ma, W. B. Zhang, L. B. Kong, Y. C. Luo and L. Kang, VO_2: from negative electrode material to symmetric electrochemical capacitor, *RSC Adv.*, 2015, **5**, 97239–97247.

35 J. Zheng, Y. Zhang, X. Jing, X. Liu, T. Hu, T. Lv, S. Zhang and C. Meng, Synthesis of amorphous carbon coated on V_2O_3 core–shell composites for enhancing the electrochemical properties of V_2O_3 as supercapacitor electrode, *Colloids Surf., A*, 2017, **518**, 188–196.

36 M. Li, G. Sun, P. Yin, C. Ruan and K. Ai, Controlling the formation of rodlike V_2O_5 nanocrystals on reduced graphene oxide for high-performance supercapacitors, *ACS Appl. Mater. Interfaces*, 2013, **5**, 11462–11470.

37 H. Pang, Y. Dong, S. L. Ting, J. Lu, C. Li, D. H. Kima and P. Chen, 2D single- or double-layered vanadium oxide nanosheet assembled 3D microflowers: controlled synthesis, growth mechanism, and applications, *Nanoscale*, 2013, **5**, 7790–7794.

38 L. Deng, G. Zhang, L. Kang, Z. Lei, C. Liu and Z. H. Liu, Graphene/VO_2 hybrid material for high performance electrochemical capacitor, *Electrochim. Acta*, 2013, **112**, 448–457.

39 M. Fu, C. Ge, Z. Hou, J. Cao, B. He, F. Zeng and Y. Kuang, Graphene/vanadium oxide nanotubes composite as electrode material for electrochemical capacitors, *Phys. B*, 2013, **421**, 77–82.

40 J. Zhu, L. Cao, Y. Wu, Y. Gong, Z. Liu, H. E. Hoster, Y. Zhang, S. Zhang, S. Yang, Q. Yan, P. M. Ajayan and R. Vajtai, Building 3D structures of vanadium pentoxide nanosheets and application as electrodes in supercapacitors, *Nano Lett.*, 2013, **13**, 5408–5413.

41 J. Liu, J. Jiang, M. Bosman and H. Fan, Three-dimensional tubular arrays of MnO_2–NiO nanoflakes with high areal pseudocapacitance, *J. Mater. Chem.*, 2012, **22**, 2419–2426.

42 J. Shi, X. Li, G. He, L. Zhang and M. Li, Electrodeposition of high-capacitance 3D CoS/graphene nanosheets on nickel foam for high-performance aqueous asymmetric supercapacitors, *J. Mater. Chem. A*, 2015, **3**, 20619–20626.

43 M. D. Stoller and R. S. Ruoff, Best Practice Methods for Determining an Electrode Material's Performance for Ultracapacitors, *Energy Environ. Sci.*, 2010, **3**, 1294–1301.

44 L. Zhang and G. Shi, Preparation of Highly Conductive Graphene Hydrogels for Fabricating Supercapacitors with High Rate Capability, *J. Phys. Chem. C*, 2011, **115**, 17206–17212.

